Assessing Flood Inundation and its impacts Using Sentinel-1A SAR Data and the Sentinel Application Platform in the Indus River Basin

Zama Mahmood[1, 2], Ghani Rahman[1, 3,*]

[1]Department of Geography, University of Gujrat, Pakistan
[2]Department of Geography and Geoinformatics, The Islamia University of Bahawalpur, Pakistan
[3]Department of Civil and Environmental Engineering, Sejong University, Seoul, Republic of Korea

[*]Corresponding author e-mail: ghani.rahman@uog.edu.pk

Received: 12 March 2026 / Accepted: 14 April 2026

Abstract. Flood disasters have become increasingly frequent and severe in Pakistan over the past few decades. In this study, Sentinel-1A Synthetic Aperture Radar (SAR) data were employed to map flood inundation and assess the damage caused by the 2022 flood in four severely affected districts of Upper Sindh, Pakistan. SAR, with its all-weather and day-and-night imaging capabilities, serves as a vital tool for timely and accurate flood damage assessment. Sentinel-1A imagery from August 28, 2022, was processed using the Sentinel Application Platform (SNAP) to capture peak inundation. Flood mapping was performed using histogram thresholding on both VV and VH polarizations, with VH polarization proving more effective in distinguishing water from land surfaces. Results revealed inundation exceeding 6,210 km², impacting over 1,928 settlements, primarily villages and hamlets. Critical infrastructure suffered major disruption, including 113 km of railway lines, 3,171 km of roadways, and 13 healthcare facilities out of 343. Agricultural losses were substantial, with rice, sugarcane, and cotton crop fields reduced by up to 50% in some areas. These findings highlight the effectiveness of SAR-based flood mapping in rapid disaster assessment, particularly in cloud-covered or inaccessible regions, and provide disaster management authorities with a reliable tool to enhance emergency response and inform future flood risk mitigation strategies.

Keywords: Flood, SNAP, SAR, Sentinel-1, Pakistan.

1. Introduction

Floods are natural catastrophes with devastating impacts and have become increasingly frequent worldwide, causing extensive loss of life and property each year (Jonkman et al., 2024; Lee et al., 2020). They are primarily driven by climatic factors such as the intensity, duration, and spatial distribution of rainfall (Bates et al., 2008; Kundzewicz et al., 2014). In addition to

meteorological causes, several physical and human factors contribute to flood occurrence and severity, including drainage density, slope, elevation, population density, soil characteristics, geology, and the presence of large reservoirs that are prone to overflow during extreme events. According to Lavell et al. (2012), floods are part of natural climatic phenomena; however, they remain a widespread and persistent threat to infrastructure, property, and human lives. The five main types of floods are flash floods, urban floods, coastal floods, glacial lake outburst floods, and riverine floods. The United Nations Office for Disaster Risk Reduction (UNDRR, 2011) reported that nearly 800 million people live in flood-prone areas, representing about 11% of the global population, with approximately 1% affected annually (Villarini et al., 2009). Over time, this number has increased to around 940 million.

In the Indo-Pak region, floods are associated with fluctuations in the summer monsoon, low-pressure systems, and interactions with western disturbances. Roxy et al. (2015) reported that warming trends in the Indian Ocean have amplified atmospheric moisture availability, resulting in more frequent and intense rainfall events and heightened flood risk. The warming trend and elevated moisture levels have increased inter-annual variability in monsoonal rainfall, characterized by a rise in short-duration, high-intensity storms (Goswami et al., 2006), which have further compounded the flood hazard across South Asia (Niyas et al., 2009). South Asian countries, particularly Pakistan, are highly susceptible to flooding due to their geographic and climatic characteristics. In Pakistan, flooding stands out as the most destructive natural hazard, causing the greatest losses in both property and human lives (Moazzam et al., 2020; Rahman et al., 2017). The global increase in climate-related disasters is evident in the Emergency Events Database (EM-DAT, 2023), which reported 387 major disaster events worldwide in 2022, resulting in 30,704 fatalities, affecting 185 million people, and causing economic losses of US$223.8 billion (CRED, 2024). Sindh province in Pakistan has experiences disastrous flooding over the last three decades, making it the most damaging natural disaster (Arif et al., 2026; Ghouri et al., 2024) due to its recurrent nature (Jamal & Rahman, 2026) and extensive damage to agriculture and infrastructure (Sarwar et al., 2025a); therefore, near-real-time monitoring and assessment have become crucial for flood management (Hafeez et al., 2026). The 2022 Pakistan floods resulted in 1,739 fatalities, affected 33 million people (Zafar et al., 2024), and caused economic losses exceeding US$15 billion, highlighting the urgent need for accurate flood monitoring and early warning systems. The transboundary Indus River system is a major water source supplying water to more than 200 million people (Zafar et al., 2026), along with its nine major tributaries, and spans approximately 1.14 million km^2 across China, India, Afghanistan,

and Pakistan. Monsoonal precipitation frequently causes the Indus River and its tributaries to overflow during the monsoon season, resulting in sustained flooding across southern Pakistan and soil erosion, posing serious challenges for farmers of the Indus basin and creating significant environmental disruption (Fahd et al., 2025). Anthropogenic drivers of these floods include uncontrolled urbanization, deforestation, encroachment on floodplains, and poor water management practices, which further aggravate the severity of flood disasters in the region (Gupta & Nair, 2011). In the monsoon of 2022, an exceptionally intense and unforeseen deluge overwhelmed the banks of the Indus River and its tributaries during August and September, resulting in sustained flooding throughout the southern regions of Pakistan. This disastrous flood rendered approximately 33 million people displaced (NDMA, 2023). Multitude contributing factors, such as intense rainfall and rapid flooding in the upper regions of the Indus basin, led to extensive inundation across the southern parts of the country. The National Disaster Management Authority (NDMA) designated 94 districts as calamity-affected, where floodwaters destroyed homes, caused severe property damage, and forced the displacement of large populations.

The basic principle behind flood inundation mapping using Synthetic Aperture Radar (SAR) involves the application of both manual and automated thresholding techniques. Threshold-based methods are widely adopted in flood mapping due to their simplicity and effectiveness (Manjusree et al., 2012). During the flood extraction process, VV and VH polarizations are commonly used, as they provide better detection of water surfaces under varying conditions (Pham-Duc et al., 2017; Sivasankar et al., 2019). Accurate identification of flood-affected areas supports disaster management authorities in predicting future flood scenarios and developing effective mitigation and response plans. The primary objective of this study is to quantify the extent of flood inundation and the impact caused by the 2022 floods in selected districts of Sindh. Traditional methods such as optical imagery analysis and ground surveys are time-consuming, labor-intensive, and often limited by weather conditions and daylight availability. These approaches also face challenges in ensuring data consistency and reliability. To address these challenges, this study employs Synthetic Aperture Radar (SAR) data, which is capable of operating in all weather conditions, both day and night. Because SAR uses radio waves that can penetrate cloud cover, it offers a reliable, high-temporal-resolution alternative for timely flood assessment and disaster monitoring.

2. Materials and Methods

2.1. Study Area

Sindh is the third largest province of Pakistan by area, covering 140,914 km^2, and the second most populous, with a population of 55.69 million according to the 2023 census. The topography of the province is predominantly flat, except in the western regions, which encompass the Kirthar Mountain Range. Historically, flooding in Sindh has been triggered by intense rainfall combined with glacial melting in northern Pakistan and Indian-administered Kashmir, which causes overflow in the Indus River and its tributaries. Areas along riverbanks, particularly near the Indus River, are most prone to flooding in Sindh, as evidenced by numerous historical flood events over the past 75 years. Sindh is traditionally divided into three climatic and geographic regions: Siro (Upper Sindh), Wichoro (Central Sindh), and Lar (Lower Sindh). Central Sindh experiences lower temperatures than Upper Sindh but higher temperatures than Lower Sindh. Southern Sindh benefits from a maritime climate, resulting in milder temperature extremes and lower rainfall than the central region. Rice, cotton, dates, and mangoes are the most commonly cultivated crops across the province. Sindh also holds ecological significance, with one national park, 16 game reserves, 10 Ramsar sites, 33 wildlife sanctuaries, three eco-regions, and 19 Important Bird and Biodiversity Areas. The province accounts for 23% of Pakistan's total population (47.85 million), with 52% residing in urban areas. The average household size is 5.55, and approximately 80% of households have access to electricity. According to the Pakistan Meteorological Department, the average annual rainfall in Sindh is approximately 160 mm, reflecting a predominantly arid environment. However, regions such as Larkana and Sukkur in Upper Sindh are susceptible to both riverine and urban flooding due to sporadic, intense rainfall events and their proximity to the Indus River. Rainfall patterns show no linear trend over time, making flood prediction difficult. Additionally, the low gradient of the Indus River and the surrounding terrain often results in impeded water flow, further exacerbating flood risks in the region. The locations of the four representative districts are shown in Figure 1.

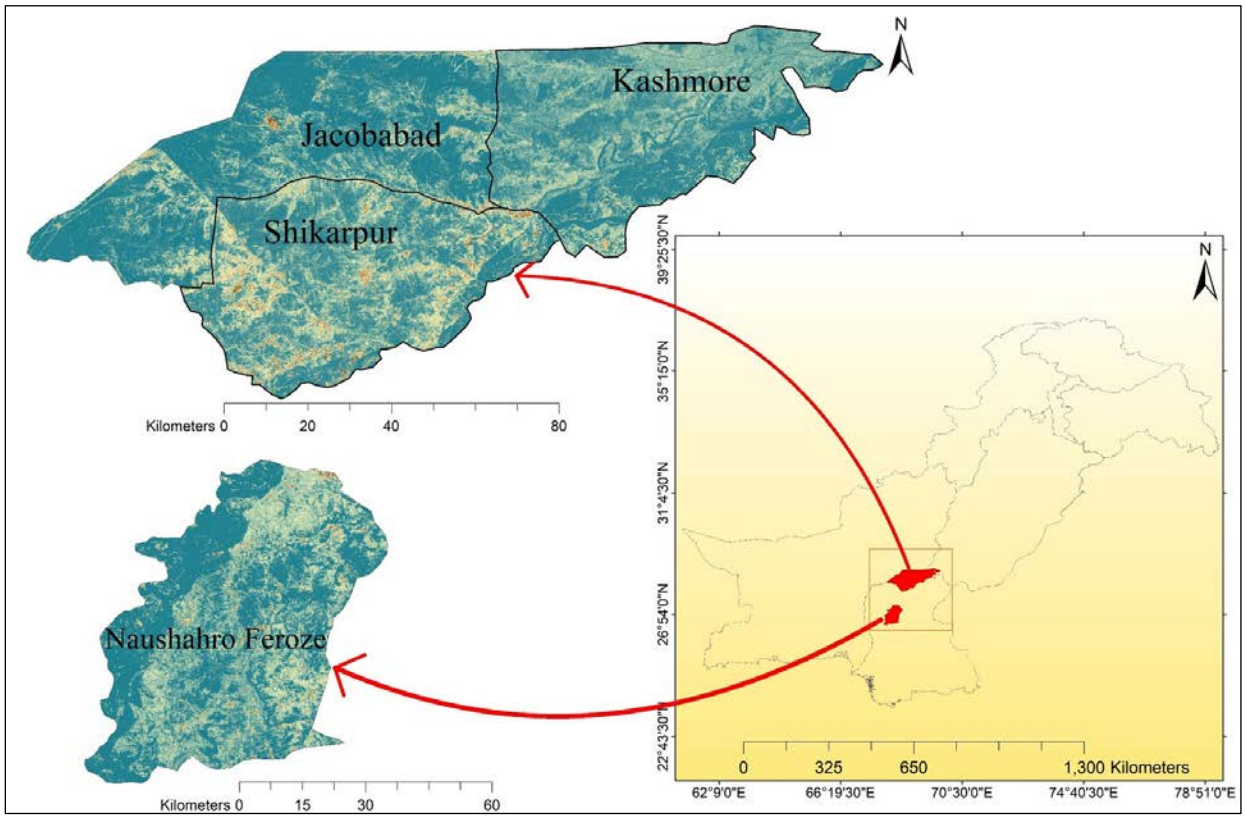

Figure 1. The Study Area

2.2. Data Acquisition

For the current study, Sentinel-1A SAR data with a spatial resolution of 5 X 20 m were acquired from the Copernicus Open Access Hub and subsequently preprocessed and analyzed using SNAP (Sentinel Application Platform). SNAP is open-source, widely used software developed by ESA for preprocessing, interpreting, and visualizing radar (microwave) data. In this study, SNAP Version 11.0 was used. Among the four acquisition modes of Sentinel-1, the Interferometric Wide Swath (IW) mode was selected, as it provides dual polarization (VV and VH) data suitable for flood mapping applications. Sentinel-1A data are available in three processing levels: Level-0 consists of raw, unfocused, and compressed data used as the base product; Level-1 includes Single Look Complex (SLC) and Ground Range Detected (GRD) products, which are ready for analysis and suitable for flood mapping; Level-2 comprises specifically processed data intended primarily for ocean-related applications such as wind, wave, and current analysis (Zeng et al., 2017). Final editing, classification, and map layout were performed using ArcGIS 10.8 and ERDAS Imagine 2015. To analyze precipitation patterns, rainfall data were obtained from the Center for Hydrometeorology and Remote Sensing (CHRS)

Data Portal (https://chrsdata.eng.uci.edu/). The CHRS Data Portal provides global rainfall estimates (with a resolution of 0.25° x 0.25°) using the PERSIANN (Precipitation Estimation from Remotely Sensed Information using Artificial Neural Networks) system, which integrates infrared satellite imagery with artificial neural network classification methods.

2.3. Preprocessing

Sentinel-1A Level-1 GRD data were first imported into the SNAP desktop application for preprocessing. In this study, ascending orbit datasets were used. The initial preprocessing step involved applying the orbit file, which incorporates the satellite's state vectors—containing information about Sentinel-1A's position and velocity relative to Earth. To obtain backscatter values, radiometric calibration was performed following orbit correction. The calibrated data were then converted into Sigma0 (σ^0) backscatter values in decibels (dB) using the following formula (Manjusree et al., 2012).

$$\sigma_{ij} = 10 \times log_{10}((DN^2 + A_0)/Aj) + 10 \times log_{10}(sin(I_j)) \quad (1)$$

where σ_{ij} is the output backscatter coefficient for scan line i and pixel j (in dB). DN is the input image value for scan line i and pixel j; $\log^{10}(\ )$ is the logarithm base 10 function; A0 is the gain offset from the first member of A_0SEG array; Aj is the gain scaling table value for column j;

sin( ) is the sine trigonometric function; and I_j is the interpolated incident angle table value for column j.

SAR systems transmit an FM chirp pulse in the range direction, described by the equation:

$$S_{pul}(t) = W_r(t).cos(2\pi f_c t + \pi k_r t^2) \quad (2)$$

In Equation 2, $S_{pul}(t)$ is the transmitted pulse as a function of time; f_c is the carrier frequency; and k_r is the Chirp rate (Romero, 2010). Upon receiving the return signal, quadrature demodulation is applied, resulting in a complex signal with both phase and magnitude. The received signal after demodulation is expressed as:

$$\mathrm{Srx}\,(\mathrm{t},\eta) = \sum_{m=0}^{M-1} \mathrm{F}\eta\mathrm{Wr}\left(t - \frac{2\mathrm{r_m}(\eta)}{c}\right) W_a(\eta - \eta_c)\mathrm{e}^{-\mathrm{j}4\pi}\left(\frac{f_0 \mathrm{R_m}(\eta)}{\mathrm{c}}\right) + \mathrm{j}\pi\mathrm{kr}\left(t - \frac{2r_m(\eta)}{c}\right)^2 + \eta_\mathrm{m}\,(\mathrm{t},\eta) \quad (3)$$

where ŋ is the azimuth time; Fŋ is the reflectivity of the target; $\frac{2r_m(\eta)}{c}$is the time delay; c is the speed of light; and W_a is the is the azimuth window function; and $\eta_m(t, \eta)$ is the additive Gaussian noise.

The next stage of preprocessing involves thermal noise removal, single-product speckle filtering, and geometric correction using the Range Doppler Terrain Correction method. Image data acquired away from the nadir position (the point directly beneath the satellite) often exhibit geometric distortions due to the satellite's viewing angle and surface topographic variations. To mitigate these distortions, terrain correction is applied, ensuring that the final image closely represents the Earth's surface with enhanced geometric accuracy. The Range Doppler Terrain Correction algorithm employs ortho-rectification techniques to convert 2D radar imagery into geocoded products, aligning the image to geographic coordinates for improved spatial accuracy. Within the SNAP toolbox, Digital Elevation Models (DEMs) with geographic coordinates (Plat, Plong, Ph) are supported. For this study, the SRTM Version 4 DEM with a 90m resolution was downloaded and utilized to provide the necessary height and elevation data for terrain correction (Fig. 2).

Satellite electronics generate heat during operation, which can introduce radiometric bias into the imagery, frequently resulting in signal distortion. Therefore, the elimination of radiometric thermal noise is an essential preprocessing step. To accurately measure backscatter, the σ^0 band function is applied, representing the radar backscatter coefficient. SAR imagery also exhibits an inherent salt-and-pepper noise pattern known as speckle, caused by the constructive and destructive interference of out-of-phase radar signals. This noise, referred to as speckle, is particularly prominent over dynamic surfaces such as moving water, where backscatter energy tends to be lower (Jensen, 2009; Lillesand et al., 2015). To mitigate this noise, the Lee filter algorithm with a 3×3 window size was applied, effectively reducing speckle while preserving critical image features and edges (Lee et al., 1994).

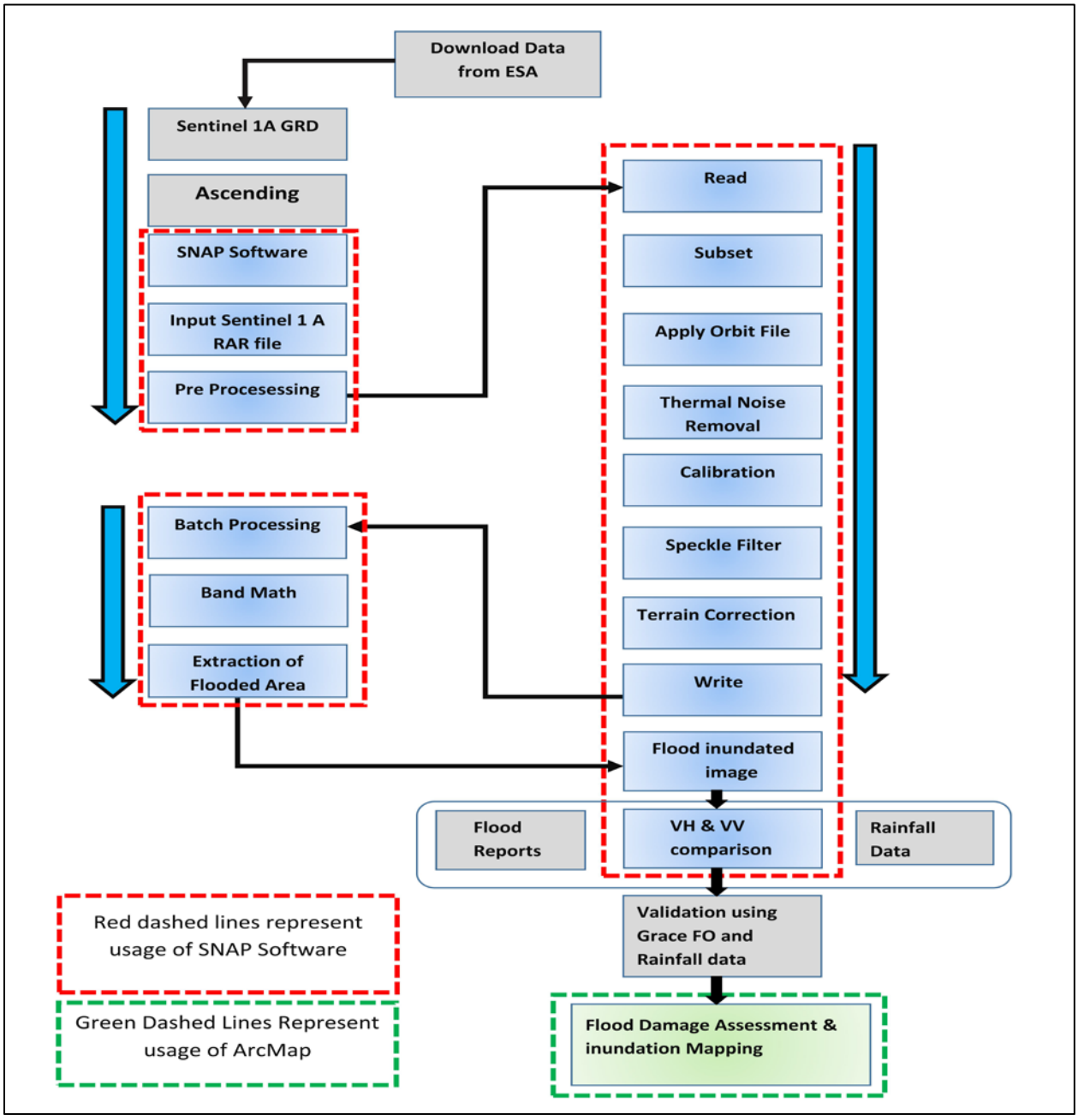

Figure 2. Data Processing Flowchart

2.4. Processing

After preprocessing, the next step involved extracting and merging segments that represent flooded areas. Lower backscatter values indicate water-covered surfaces, whereas higher values correspond to non-water features such as land, vegetation, or built-up areas. This study employed histogram-based thresholding as the primary segmentation technique, which is recognized for its simplicity and effectiveness in classifying radar images (Hong et al., 2015; Xia et al., 2011).

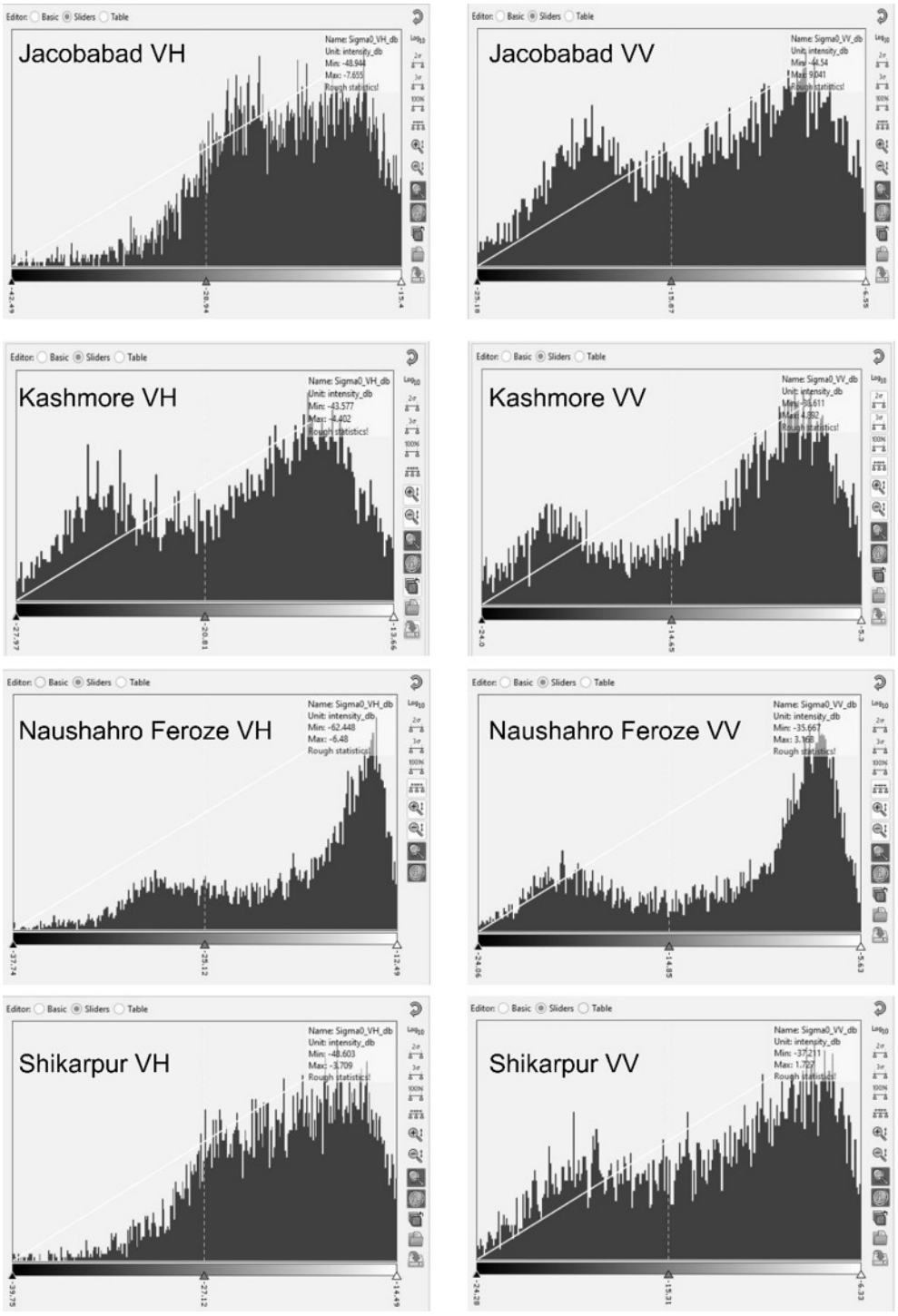

Figure 3. Histogram Values of VH and VV Polarization. Smooth surfaces typically produce specular reflection and low backscatter, whereas rough surfaces generate high backscatter and strong radar returns

A comparison of different filtering techniques—Refined Lee, Lee 3x3, Lee 5x5, and Sigma Lee—was conducted on radar images using VH and VV polarization (Fig. 4).

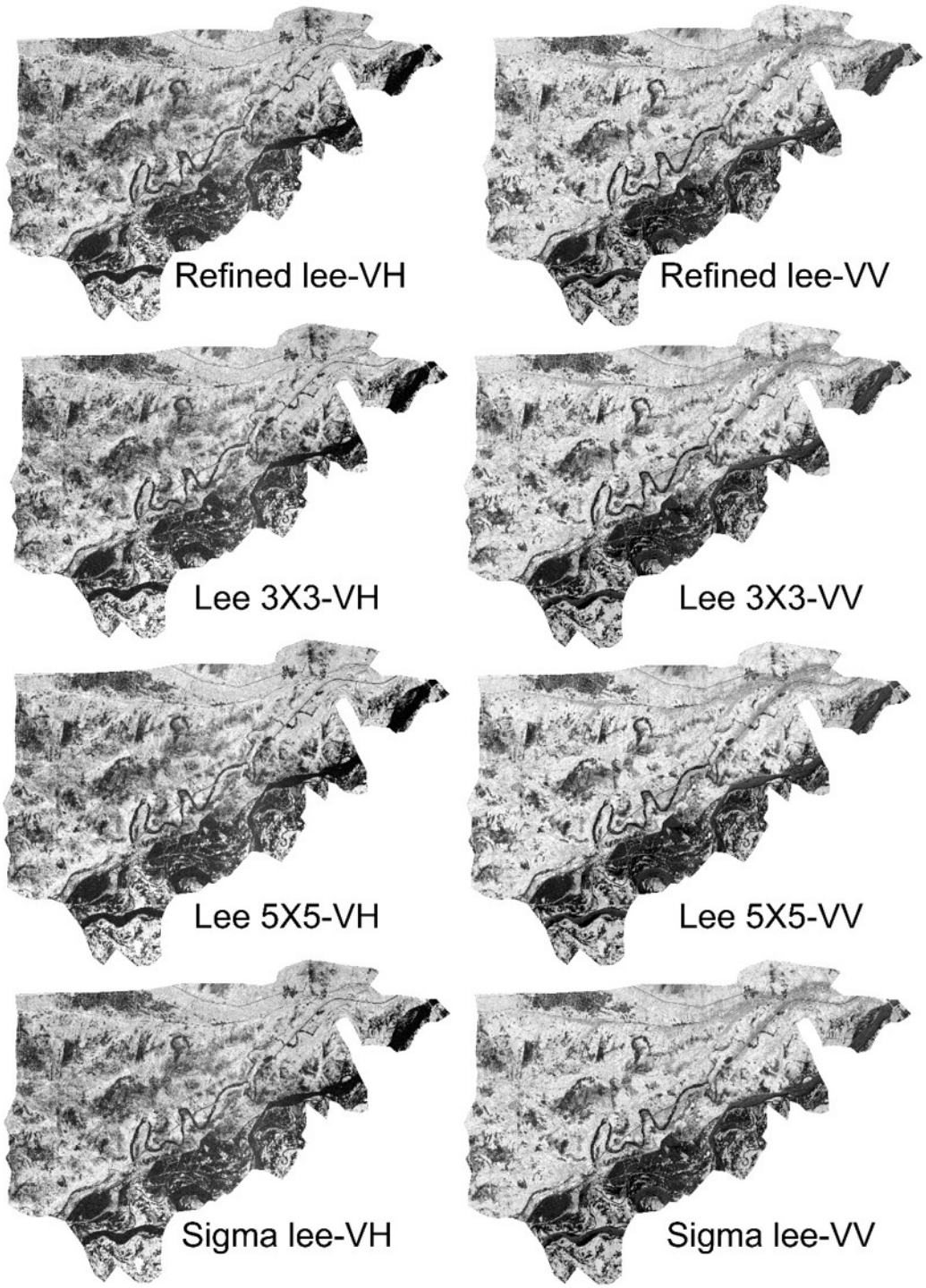

Figure 4. Comparison of Different Filters Showing VH and VV Polarization. Once all processing steps are completed, the final output is presented as binary data, enabling a clear distinction between flooded and non-flooded areas

These filters improve flood mapping accuracy by reducing noise while preserving important image details. Speckle noise is a common issue in radar imagery and can obscure key features, making it challenging to differentiate between flooded and non-flooded areas. Filtering methods such as the Lee and Sigma Lee filters enhance image clarity by removing noise, thereby

improving the accuracy of flood boundary delineation. Additionally, polarization plays a significant role in flood detection, with VH polarization providing better contrast between water and land surfaces than VV polarization. Smaller kernel sizes, like Lee 3x3, retain finer details but may leave residual noise, while larger kernel sizes, such as Lee 5x5, provide stronger smoothing but at risk of losing subtle features. These refined radar images enable researchers to develop high-precision flood extent maps and contribute to more effective disaster response strategies. These techniques support better risk assessment and mitigation planning, ultimately enhancing community resilience in flood-prone areas.

3. Results

3.1. Pre and Post flood VH and VV polarization Analysis

The study utilized two sets of SAR images: the pre-flood images had sensing time of 2022-05-26 1:25:44, 2022-05-30 13:28:19.0, 2022-05-26 01:25:19, while the flood-period images had sensing time of 2022-08-30 1:25:51, 2022-09-03 13:28:25 and 2022-09-06 01:17:09 respectively. Figure 5 illustrates the pre-flood conditions using VH and VV polarization, whereas Figure 6 shows the post-flood conditions with the same polarization modes. In the pre-flood imagery, water remained contained within the banks of the Indus River (Fig. 5). The disparity between flooded and non-flooded scenes formed the basis for determining threshold values, which varied across images. The floodwater reached its maximum extent on 28 August in the Kashmore, Jacobabad, Shikarpur, and Naushahro Feroze districts, damaging agricultural fields and infrastructure. Figure 6 illustrates the extent of inundation. The findings reveal that most of the area on the western side of the Indus River was inundated due to lower elevations toward the Kirthar Mountain Range, while the adjacent areas along the river also experienced significant flooding. It is evident in Figure 5 that VH and VV polarizations produce different results, with VH polarization offering higher sensitivity for class separability. This enhanced separability is visible in both the preprocessed images and the binary classifications (Figs 5 and 6). Due to intense rainfall, flood defenses and levees were at risk of structural failure; and previous studies indicate that when water levels exceed a critical threshold, riverbanks tend to collapse under hydraulic pressure.

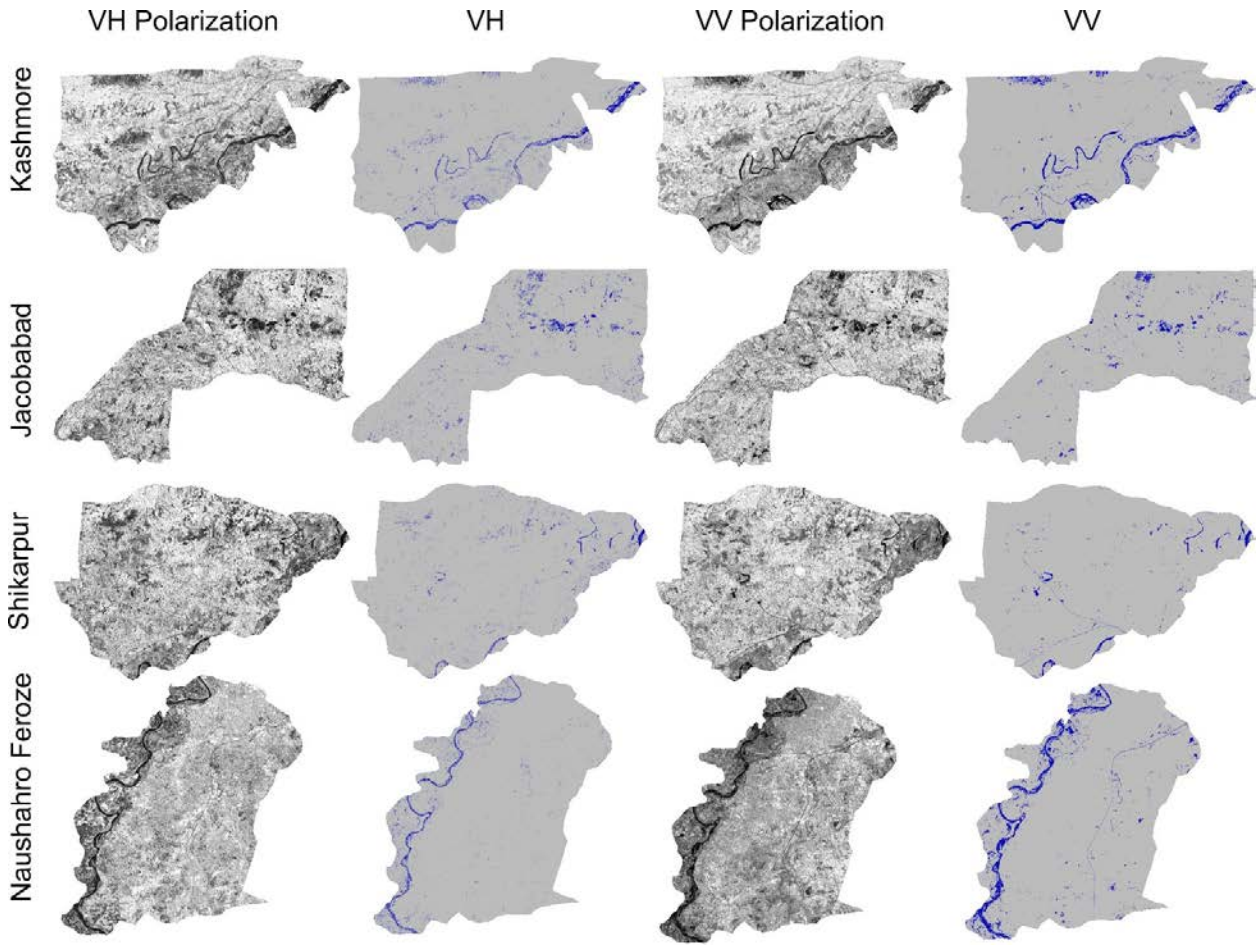

Figure 5. Comparison of VH and VV Polarization before the flood, after applying threshold values

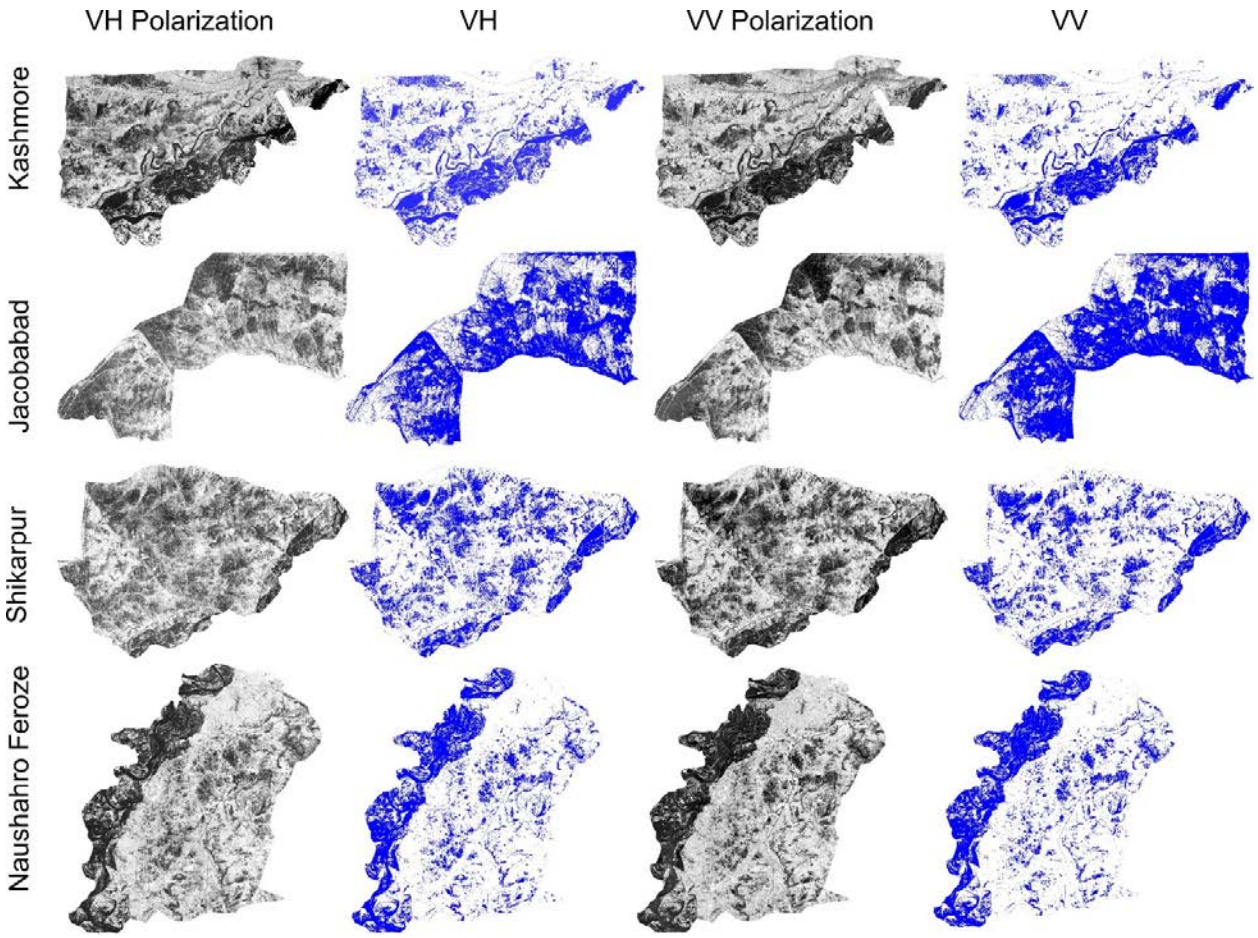

Figure 6. Four sites showing VH and VV polarization in the post-flood condition after applying threshold values to delineate inundated areas

The 2022 flood in Pakistan resulted from persistent wet spells, causing significant economic damage. Hydro-meteorological analysis shows that peak rainfall occurred in August, reaching 438.99 mm. During the same period, parts of southern Punjab and the Sindh divisions of Larkana, Sukkur, and Shaheed Benazirabad experienced considerable overland flow from the foothills of the Kirthar Mountain Range, which further amplified flood magnitude. Figures 5 and 6 demonstrate that Synthetic Aperture Radar (SAR) is highly effective for detecting and delineating floodwater under all weather conditions. The areas submerged in Kashmore, Jacobabad, Shikarpur, and Naushahro Feroze districts were 1,118.38, 2,144.348, 1,703.40 and 1,244.052 km^2, respectively. The spatial analysis also reveals that maximum flooding occurred at elevations between 45.72 and 57.91 m above sea level, highlighting the influence of local topography on floodwater accumulation.

The PERSIANN rainfall data show that maximum precipitation occurred in August, as illustrated in Figure 7. The figure shows the rainfall distribution across Pakistan during 2022, clearly highlighting the unusually high monsoonal rainfall during August. Most regions of the

country, including Sindh province, experienced a substantial amount of rainfall during August. Hydro-meteorological analysis indicates that the 2022 flood resulted from twelve consecutive weeks of wet spells, beginning in June and peaking in August, when 438.99 mm of rainfall was recorded in parts of Sindh and Balochistan. This prolonged and intense precipitation was preceded by extreme heatwaves from March to May, during which temperatures exceeded 51°C in southern Pakistan. These conditions strengthened a persistent low-pressure system, intensifying monsoonal depressions and producing exceptionally heavy rainfall. Several studies have investigated the relationship between climatic variables and flood events, but results consistently show no significant correlation between temperature and rainfall during major floods. In 2010, a weak negative correlation was reported ($p = 0.02$, $r = -0.06$), while in 2022, the association remained non-significant ($p = 0.91$, $r = -0.09$) (Nazli et al., 2025). Similarly, wind speed exhibited no significant correlation with temperature in 2022 ($p = 0.95$, $r = 0.05$), reflecting evolving thermodynamic processes and reduced moisture transport (Nazli et al., 2025). In contrast, rainfall and atmospheric pressure demonstrated a significant positive correlation both in 2010 ($p = 0.03$, $r = 0.63$) and 2022 ($p = 0.04$, $r = 0.55$). The 2010 floods were associated with a strong low-pressure system that prevailed over northern Pakistan, whereas in 2022 a weaker but comparable system developed over southern Pakistan, indicating a shift in monsoonal dynamics (McBride & Nicholls, 1983).

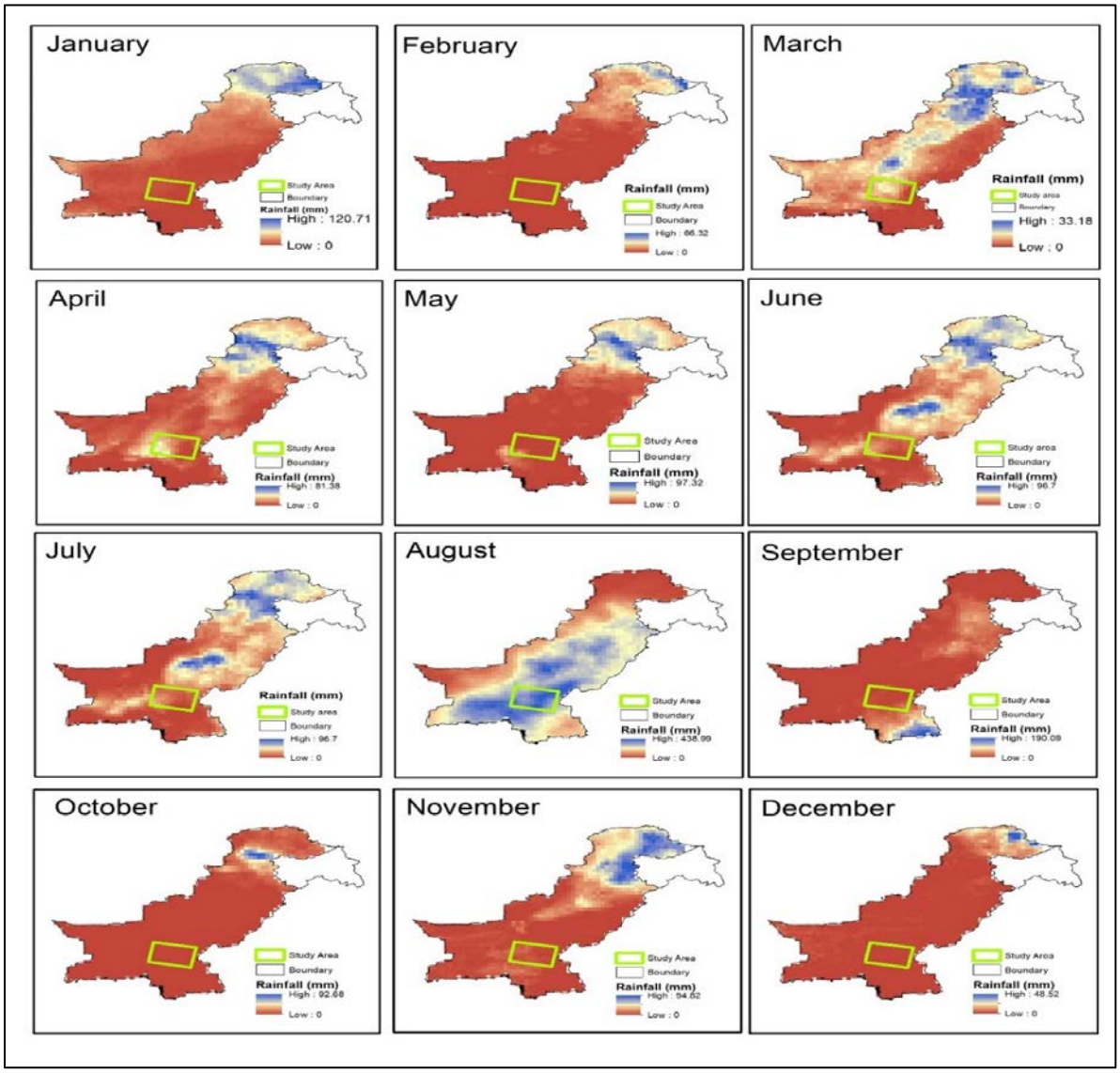

Figure 7. Monthly rainfall patterns in Pakistan for 2022

Grace-FO satellite observations further confirm the severity of the 2022 flooding. A pronounced peak in Water Equivalent Thickness (WET) was recorded in August 2022 (Fig. 8), capturing dramatic increases in surface water, soil moisture, and groundwater storage. This surge reflects extensive inundation, deep soil saturation, and enhanced groundwater recharge. The prolonged elevation in WET indicates extended floodwater retention, saturated floodplains, and delayed flood recession, all of which contributed to infrastructure damage and prolonged recovery challenges for affected communities.

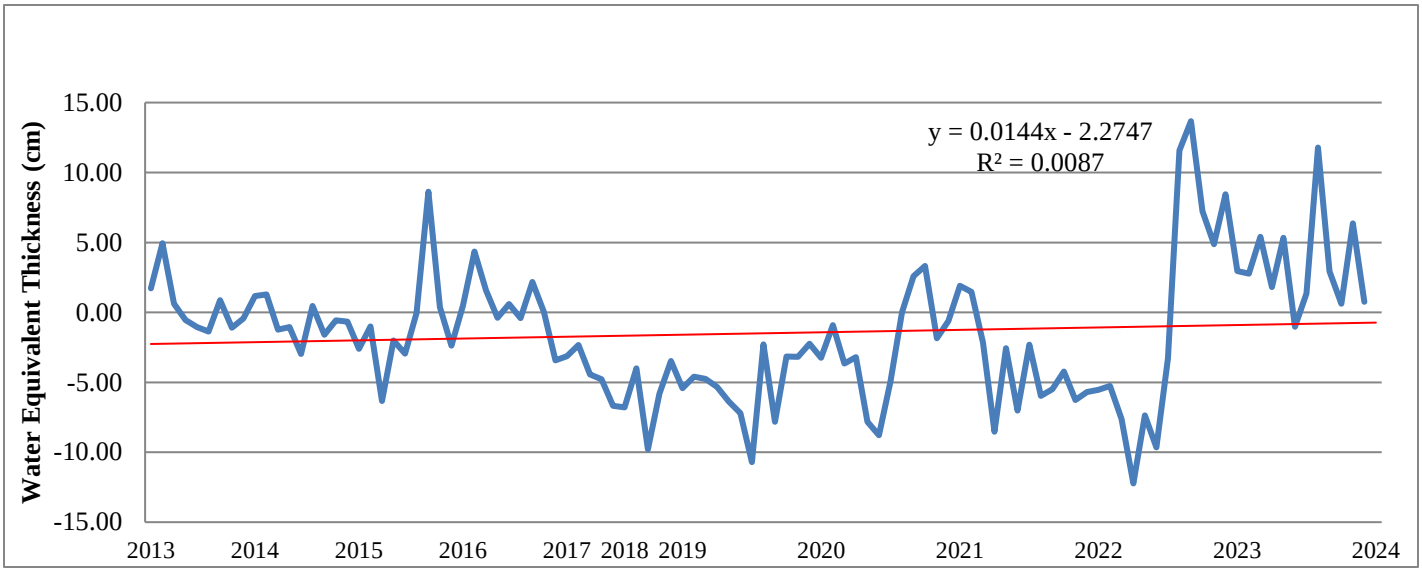

Figure 8. GRACE-FO Monthly Water Equivalent Thickness

3.2. Impacts of Flood on Various Sectors

3.2.1. Impact of Flood on Agriculture

Following the collection of spatial data before and after the flood across all four districts, the resulting statistics were compiled to illustrate both the magnitude of damage and the scale of agricultural devastation (Fig. 9). Flooding is the most severe natural hazard affecting the Indus Basin, where livelihoods predominantly depend on crop cultivation. The analysis of pre- and post-flood spatial data clearly shows that all four districts experienced substantial agricultural losses, emphasizing the vulnerability of major crops such as rice, sugarcane, and cotton. Before the 2022 flood, the total cultivated area in Kashmore was 1,711 km² (746.4 km² of cropland), with rice and sugarcane as the dominant crops. Rice occupied 1,051.19 km² before the flood, which declined to 1,033.41 km², indicating that 17.78 km² of rice fields were submerged. Sugarcane was cultivated over 12.17 km², of which 2.16 km² was destroyed. Kashmore had a total flooded agricultural area of 1,311 km², representing 76.65% of cultivated land (Table 1).

Table 1. Impact of the 2022 Floods on Agricultural Crops in Four Selected Districts

District Name	Total Agricultural Area (km^2)	Flooded Tree Orchard Area (km^2)	Flooded Agricultural Area (km^2)	Flooded Agricultural Area (%)
Kashmore	1,711	3	1,311	76.65
Jacobabad	2,056	1	1,919	93.12
Shikarpur	1,788	11	1,462	81.72
Naushahro Feroze	2,245	216	543	24.21

Source: Mushtaq et al. (2022).

In Jacobabad, the total cropland area was 2321.6 km², with rice covering 1,280.35 km² before the flood. After inundation, the flooded rice area amounted to 949.92 km², representing one of the largest single-district agricultural impacts in Sindh. Sugarcane losses were measured at 6.65 km² (Table 2). Jacobabad recorded the highest agricultural flooding percentage at 93.12% (Table 1). The climate of Sindh is notably conducive to a limited range of crops, which serve as the primary source of income for the rural population. Sugarcane, recognized as the second most significant crop in Sindh, is a profitable commodity for farmers and is eagerly anticipated each season. The extensive losses highlight the vulnerability of these crops, which require specific hydro-meteorological conditions and high input costs.

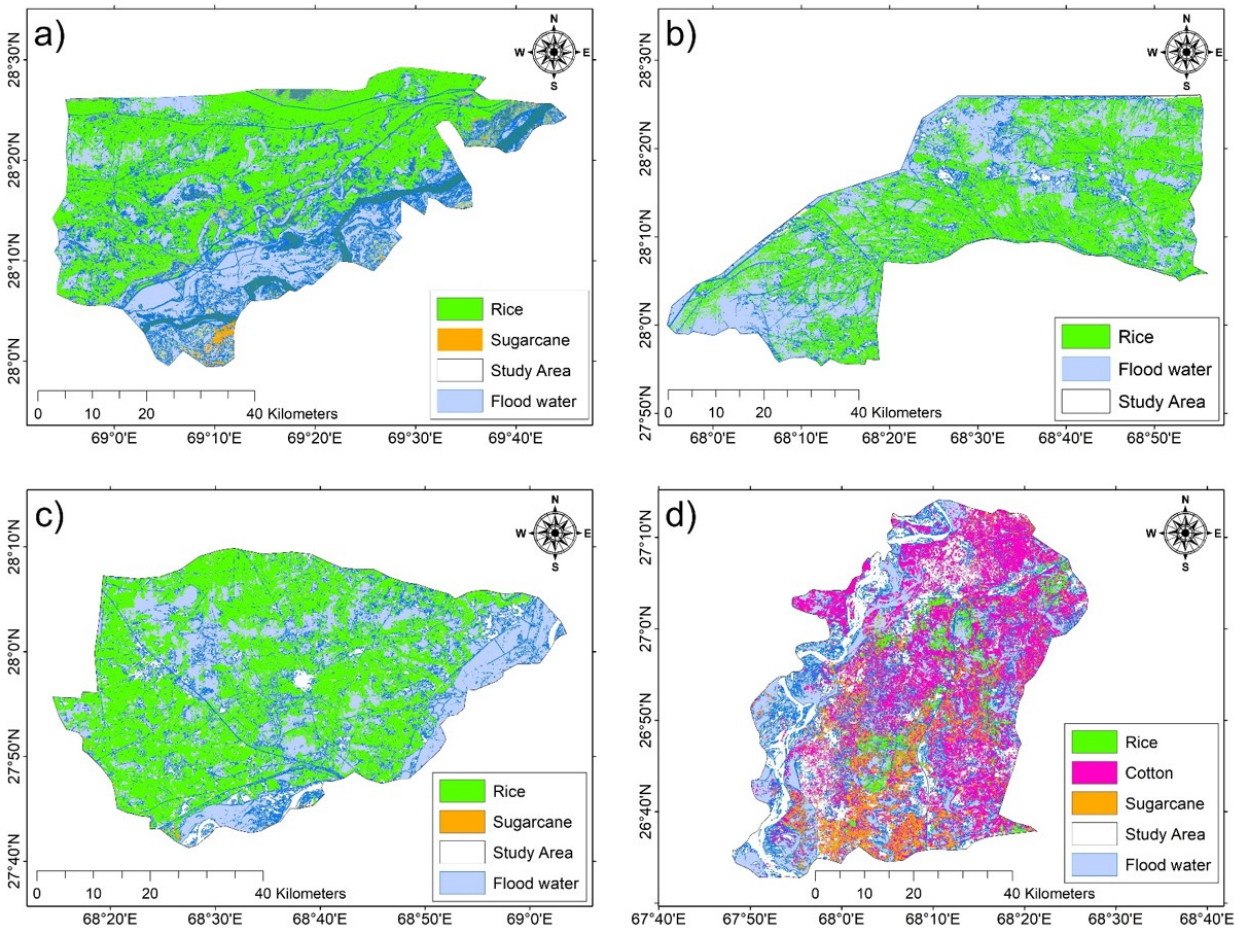

Figure 9. Impact of the 2022 floods on Agricultural crops in four districts: (a) Kashmore, (b) Jacobabad, (c) Shikarpur, (d) Naushahro Feroze

In Shikarpur, with 2,576.59 km² of total land and 2034.3 km² of cropland, approximately 55% of agricultural land was affected. Rice cultivation covered 1,248.35 km² before the flood, of which 745.91 km² was inundated, leaving 502.44 km² viable. Sugarcane declined from 2.26 km² to 1.43 km². Shikarpur had 1,462 km² of total flooded agricultural land. All 54 union councils in the district were affected by flooding. Among the four selected sites, Shikarpur recorded the second-highest rice cultivation with 1,248.35 km² with a mean yield of 3,745 Kg/Acre before the flood. However, 745.91 km² of cultivated rice area was inundated, leaving only 502.44 km² viable. This was one of the largest absolute losses of rice cultivation area in the study region during the 2022 flood, severely affecting food production and local supply chains. Sugarcane, cultivated across 2.26 km² before the flood, declined to 1.43 km² afterward. The combined effect of these agricultural losses is particularly critical in Sindh, where rice and sugarcane are not only staple crops but also constitute primary economic resources for farmers. The 2022 flood had cascading consequences, affecting both food security and household income.

Naushahro Feroze district, with an area of 3,025.48 km² and 2412.3 km²of cropland, suffered 24.21% flooding. All 68 union councils in the district were affected; however, the northwestern and southeastern union councils were relatively less impacted. During peak inundation, 62 villages were completely submerged, and 2,631 villages were surrounded by water, making navigation impossible by conventional means. Agricultural diversity was higher here, with rice, sugarcane, and cotton cultivated in substantial areas. Cotton dominated cultivation with 936.39 km², but this decreased to 592.42 km² after the flood, meaning 36.64% of cotton area was destroyed (Table 2). Sugarcane declined from 268.05 km² to 48.64 km², and rice cultivation declined from 140.83 km² to 74.49 km². This level of damage has broader implications, as surrounding districts such as Ghotki, Tando Adam, Thatta, Tando Allah Yar, Mirpur Khas, Tando Muhammad Khan, Sanghar, Badin, and Sukkur contribute significantly to sugarcane production in Sindh, each producing more than 100,000 tons annually.

Table 2. Before and after flood inundation status of crops

District	Crops	Post-Flood Cultivated Area (km^2)	Flood Inundated Area (km^2)	Yield (Kg/Acre)
Kashmore	Rice	1051.19	17.782	3645
	Sugarcane	12.17	2.1624	26000
Jacobabad	Rice	1280.350	949.924	3735
Shikarpur	Rice	1248.351	745.91	3745
	Sugarcane	2.2634	1.43	17220
Naushahro Feroze	Rice	140.83	74.489	3745
	Sugarcane	268.0549	48.635	17260
	Cotton	936.39	343.9795	1567

All four districts illustrate how the 2022 floods inflicted widespread damage on agricultural systems in Sindh. Both rice and sugarcane, essential for subsistence and cash income, were heavily impacted across all sites, with losses ranging from 15% to nearly 74%. Cotton, grown extensively at Naushahro Feroze, suffered a reduction of almost 36% reduction in cultivated area. Beyond immediate reductions in cultivated land, the floods also disrupted yield potential, with expected harvest per acre significantly declining due to waterlogging, siltation, and delays in replanting. These results show the dual vulnerability of agriculture in Sindh: the physical exposure of crops to extreme flooding events and the economic fragility of farming communities reliant on a narrow set of crops. The inundation of large tracts of agricultural land not only

reduced the cultivated area but also threatened food availability, farmer livelihoods, and the stability of regional markets.

Beyond agricultural losses, the 2022 flood also resulted in significant environmental and livestock impacts across all four districts. Forest areas were severely affected by flooding (Table 3). Naushahro Feroze had the largest total forest area at 153.27 km², yet experienced relatively lower flood impact, with 25.46 km² inundated (16.6% loss). In contrast, Jacobabad, despite having only 57.37 km² of total forest, lost 39.48 km² to flooding, representing the highest percentage loss at 68.8%. Similarly, Shikarpur lost 42.33 km² out of 87.16 km² (48.6%), and Kashmore lost 37.15 km² out of 72.44 km² (51.3%). Across all four districts, a total of 144.42 km² of forest area was inundated. These forest losses have significant ecological implications, affecting biodiversity, carbon sequestration, soil stabilization, and watershed management.

Table 3. Flooded Forest Area

District Name	Total Forest Area	Tree Sparse Forest Area (Km^2)	Dense Forest Area (Km^2)	Flooded Sparse Forest Area (Km^2)	Flooded Dense Forest Area (Km^2)	Total Flooded Forest Area (Km^2)	Livestock Perished
Kashmore	72.44	53.03	19.41	30.22	6.93	37.15	24,201
Jacobabad	57.37	54.75	2.63	38.27	1.2	39.48	15,680
Shikarpur	87.16	76.26	10.9	39.47	2.86	42.33	7,802
Naushahro Feroze	153.27	134.1	19.17	21.1	4.36	25.46	36,588

Source: Mushtaq et al. (2022).

3.2.2. Flood Impacts on Settlements, People, and Public Services

In Kashmore district, there were 1,339 communities of varying sizes, of which 289 were entirely submerged by floodwater. Kashmore district comprised of three major towns—Kashmore, Tangwani, and Bakshapur—and one major city, Kandhkot, covering a total area of 2,549.03 km². According to the Provincial Disaster Management Authority Rehabilitation Centre, 31, 31, 111, and 85 deaths were reported in Kashmore, Jacobabad, Shikarpur, and Naushahro Feroze, respectively, making Shikarpur the district with the highest number of fatalities among the four selected districts. Similarly, 35 people in Jacobabad, 124 in Shikarpur, and 61 in Naushahro Feroze were injured. On 29 August 2022, 47 villages in Kashmore were completely submerged, while 916 villages were surrounded by floodwater, which persisted for up to four months in some parts of the district, indicating the widespread severity of inundation. The flood had an

immense humanitarian impact, disrupting population distribution, settlement accessibility, and livelihood security across all four districts. In Kashmore, out of the total population of 1,233,957, approximately 679,756 people were affected, and 112,479 households suffered damage. Similarly, 545,230 people in Jacobabad, 400,000 in Shikarpur, and 234,168 in Naushahro Feroze were affected due to flooding and displacement (Table 4).

In addition to the submerged villages, 1,154 villages across the study area were surrounded by floodwater, making access impossible by conventional transportation. A spatial analysis of Jacobabad district further confirmed that all 42 union councils were affected. The total numbers of households affected in Jacobabad, Shikarpur, and Naushahro Feroze were 97,854, 96,000, and 70,372, respectively. A large number of houses were also partially or fully damaged due to prolonged exposure to floodwater and structural fragility. The number of partially damaged houses was 32,027 in Kashmore, 24,073 in Jacobabad, 19,047 in Shikarpur, and 43,688 in Naushahro Feroze. Fully damaged houses totaled 44,540 in Kashmore, 89,784 in Jacobabad, 72,212 in Shikarpur, and 105,110 in Naushahro Feroze. According to the Works and Services Department of Sindh, 40 union councils in Kashmore, 44 in Jacobabad, 55 in Shikarpur, and 68 in Naushahro Feroze were affected. Additionally, one bridge in Kashmore and two bridges in Naushahro Feroze were damaged, along with 14 culverts in Kashmore and 124 culverts in Naushahro Feroze.

Table 4. Settlement Inundation, Population Affected and Human Losses

District	Total Settlements	Inundated Settlements	Population Affected	Households Affected	Deaths	Injuries
Kashmore	1339	289	679,756	112,479	31	–
Jacobabad	1922	804	545,230	97,854	31	35
Shikarpur	1405	436	400,000	96,000	111	124
Naushahro Feroze	2286	399	234,168	70,372	85	61

Source: Sindh (2022).

Across the four districts, 2,548 government buildings suffered damage, disrupting essential administrative and public services. Health sector infrastructures were also affected by the flood. Although only one BHU (Motan Mehar) in Kashmore was fully submerged, many health facilities across the four districts experienced partial inundation, structural damage, or severe accessibility constraints (Table 5). Jacobabad reported the highest number of affected health facilities, with eight facilities, including five BHUs and one General Hospital, impacted on 28 August 2022. Shikarpur recorded four BHUs inundated, while Naushahro Feroze experienced

major access disruptions as surrounding floodwaters cut off road connections to several health facilities.

Table 5. Health Facilities and Flood-Affected Infrastructure

District	Civil Hospital (#/beds)	Dispensaries	RHC (#/beds)	TB Clinics	BHUs (#/beds)	MCHC (#/beds)	Facilities Affected
Kashmore	2/54	34	4/24	8	27/56	2/2	1 BHU
Jacobabad	3/231	6	3/24	9	20/40	16/67	8 Health facilities
Shikarpur	2/331	16	9/126	9	37/70	5/0	4 BHUs
Naushahro Feroze	3/147	50	13/88	15	45/90	–	Access to Health Facilities disrupted

Source:Sindh (2022).

Understanding the pre-flood health service usage helps contextualize the severity of the disruption caused by the 2022 flood. The indoor and outdoor patient data for 2021 show that Naushahro Feroze had the highest outpatient load at 2,231,761, followed by Shikarpur (1,184,525), Jacobabad (1,126,946), and Kashmore (609,310) (Table 6). These large patient volumes indicate a heavy dependence on local health facilities, which were subsequently disrupted during the flood.

Table 6. Total Indoor and Outdoor Patient Data

District	Indoor Male	Indoor Female	Total Indoor	Outdoor Male	Outdoor Female	Total Outdoor
Kashmore	2,643	3,036	5,679	285,699	323,611	609,310
Jacobabad	17,621	22,196	39,817	484,954	641,992	1,126,946
Shikarpur	11,510	13,911	25,421	486,579	697,946	1,184,525
Naushahro Feroze	15,970	18,329	34,299	1,008,897	1,222,864	2,231,761

Figure 10 illustrates the spatial distribution of flood impacts on multiple assets. In Kashmore district, most settlements lie on the north-western side of the Indus River, and as floodwaters expanded, these settlements became disconnected from communities on the eastern side, severely affecting mobility and access to essential services. Jacobabad district, located on the north-western edge of Sindh and bordered by the Sulaiman Mountain Range, faced substantial inundation. Among its 1,922 settlements, 804—mostly villages and small settlements—

experienced severe flooding. The district has a total area of 2,769.36 km² with 2321.6 km² of cropland. Jacobabad had 111 health facilities, including 39 BHUs, 9 General Hospitals, and 3 RHCs, with eight health facilities affected during the flood. Shikarpur, with a population of 1,386,330 and covering 2,576.89 km², is predominantly an agricultural district. Out of 1,405 settlements, 436 were inundated, causing substantial social and economic disruption. Shikarpur had 97 health facilities, including 60 BHUs, one DHQ Hospital, and 14 General Hospitals, with four BHUs inundated. Shikarpur also has three railway stations—Habibkot Junction, Shikarpur, and Sultankot—that experienced service disruptions due to the flood. In Naushahro Feroze, 2,286 settlements were identified, of which 399 were submerged. The district has three major urban centers—Naushahro Feroze, Moro, and Kandiaro—and two railway stations. A total of 73 health facilities were present, including 7 BHUs, 9 General Hospitals, and 5 RHCs. Although none of the major health facilities were fully submerged, access to many was blocked until October by surrounding floodwaters, severely disrupting healthcare delivery.

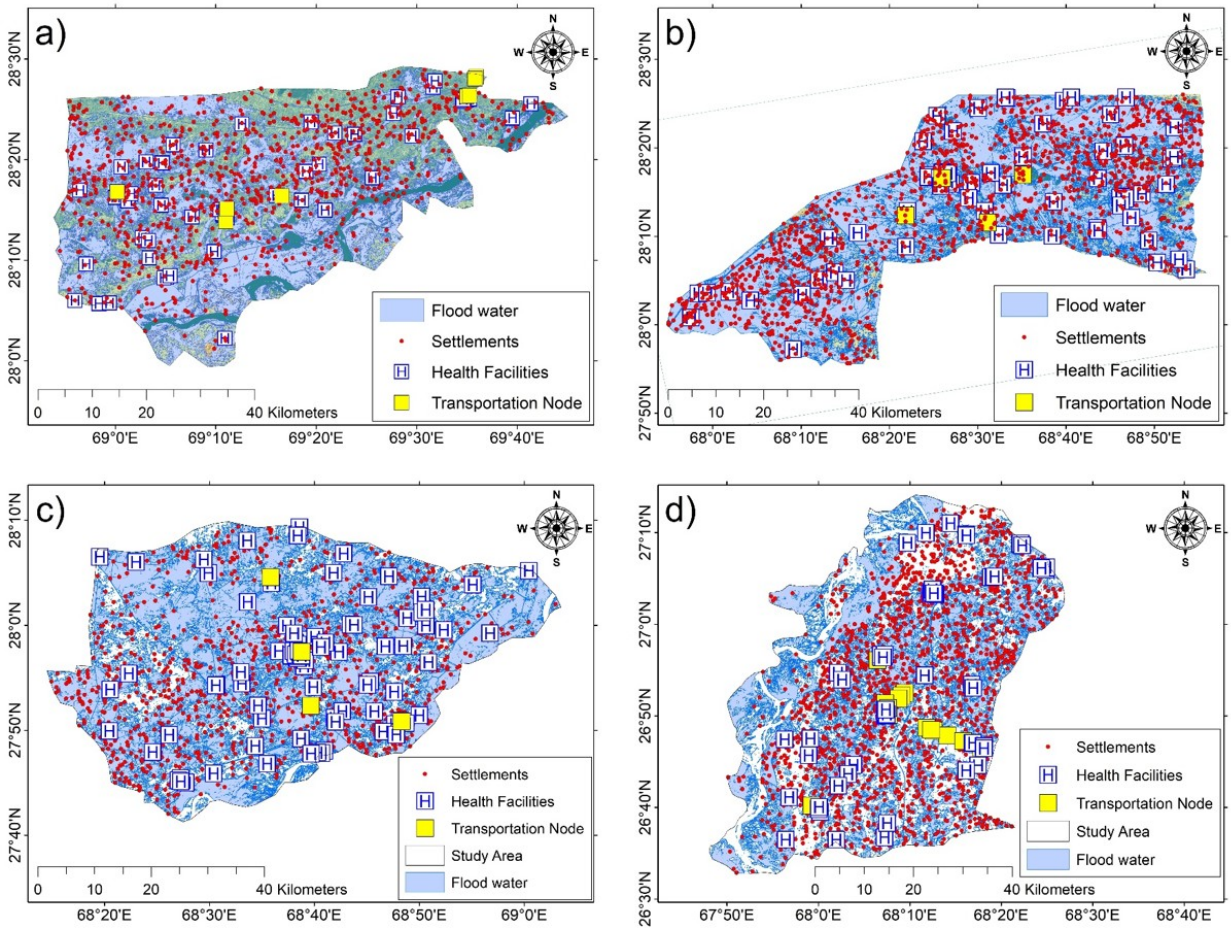

Figure 10. Flood Impacts on Settlements and Public Services: (a) Kashmore, (b) Jacobabad, (c) Shikarpur, (d) Naushahro Feroze

3.2.3. Impact of the 2022 Flood on the Transportation Network

A 74.98 km railway line originates from the north-eastern side of Kashmore and extends toward the south-western part of the district, of which 17.78 km were submerged during the 2022 flood (Table 7). Similarly, out of Kashmore's 2,095.42 km road network, 359.87 km of roads were inundated, disrupting the movement of people and goods and isolating several settlements. In Jacobabad district, a total of 133.18 km of railway line extends from the northern part of the district to its southwestern side. During the peak flood period, 64.27 km of this railway corridor was completely submerged. Out of four railway stations in Jacobabad, two remained non-functional due to prolonged inundation, as multiple sections of track remained underwater. The situation for the road network was equally severe: out of 2,654.05 km of total road length, 1,042.09 km were submerged, indicating a massive disruption to intra-district and inter-district connectivity. Shikarpur contains a 3,056.90 km road network connecting 1,405 settlements across both sides of the Indus River. After the August 2022 flood, 964.43 km of roads remained inundated. Similarly, a total of 85.84 km of railway line traverses Shikarpur, of which 22.82 km was submerged. This extensive damage hindered the movement of relief goods and emergency medical support. Naushahro Feroze has an extensive road network measuring 3,710.35 km and 107.68 km of railway line. Following the 2022 flood, 804.83 km of roads and 8.21 km of railway line were completely submerged, significantly affecting mobility, supply routes, and access to health facilities.

Table 7. Flood Inundation of Transportation Networks

District / Site	Total Railway Line (km)	Railway Line Submerged (km)	Total Road Length (km)	Road Length Submerged (km)
Kashmore	74.98	17.782	2095.42	359.87
Jacobabad	133.178	64.27	2654.05	1042.09
Shikarpur	85.84	22.82	3056.9	964.43
Naushahro Feroze	107.682	8.205	3710.35	804.83

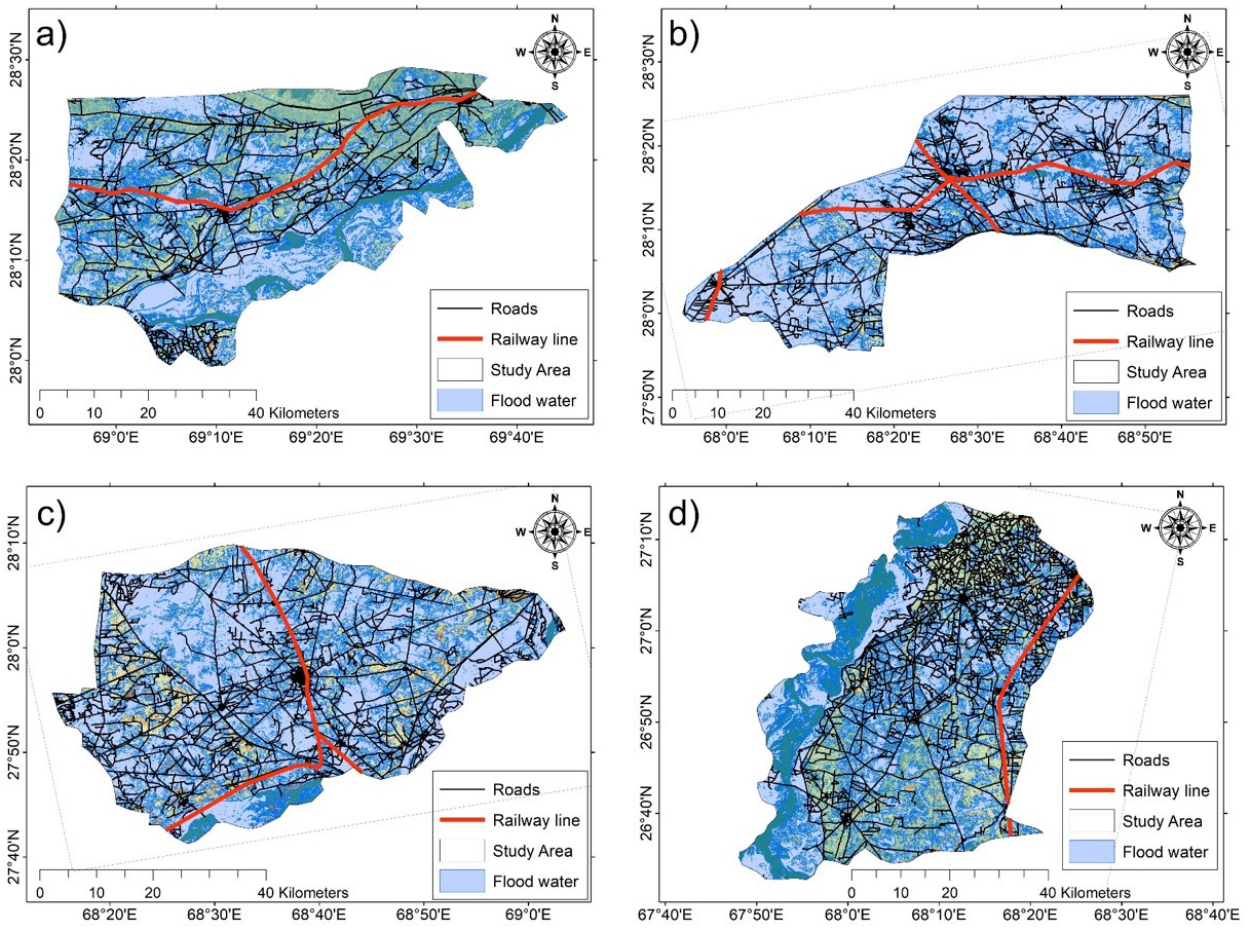

Figure 11. Impact of flood on Transportation networks: (a) Kashmore, (b) Jacobabad, (c) Shikarpur, (d) Naushahro Feroze

4. Discussion

This study utilized Sentinel-1A SAR data processed through SNAP to assess flood inundation across four severely affected districts in Upper Sindh: Kashmore, Jacobabad, Shikarpur, and Naushahro Feroze, during the July-August 2022 flood. The Sentinel-1A imagery acquired on 28 August 2022, representing peak flood conditions, was processed using histogram-based thresholding applied to VH and VV polarizations. VH polarization demonstrated superior performance in water-land discrimination, providing better contrast than VV polarization, and similar findings have been reported in previous studies (Clement et al., 2018; DeVries et al., 2020).

The speckle filter was applied to reduce coherent interference noise. The Lee filter (3×3 kernel) was employed for both polarizations, enhancing smoothness while preserving edges and spatial resolution (Argenti et al., 2013; Lee et al., 1994). The histogram-based thresholding

method, recognized for its computational efficiency, was applied after orbit correction, radiometric calibration, thermal noise removal, and terrain correction using SRTM DEM (Manjusree et al., 2012; Twele et al., 2016). Histogram analysis revealed a characteristic bimodal distribution: the lower peak corresponded to water (< -15 dB for VH), while the higher peak represented non-flooded regions (> -10 dB).

The spatial analysis revealed extensive flooding: Kashmore (1,118.38 km²), Jacobabad (2,144.35 km²), Shikarpur (1,703.40 km²), and Naushahro Feroze (1,244.05 km²), with maximum inundation observed in areas situated between elevations of 45.72 to 57.91 m above sea level. The flood inundated 1,928 settlements out of a total of 6,952, affecting 1,859,154 people and causing 258 fatalities across the four districts. Province-wide, total fatalities in Sindh were 1,093, with 8,422 injuries (PDMA Sindh, 2022). Housing damage was catastrophic: 311,646 houses were fully damaged and 118,835 partially damaged. Transportation infrastructure sustained extensive damage: 113.08 km of railway line were submerged and 3,171.22 km of roads were inundated, severely disrupting mobility and emergency response. Agricultural losses were severe, with a total of 5,235 km² affected. District-level impacts varied: Kashmore (76.65% of agricultural land flooded), Jacobabad (93.12%), Shikarpur (81.72%), and Naushahro Feroze (24.21%) (Mushtaq et al., 2022). Rice cultivation sustained 1,788.09 km² losses, with Jacobabad experiencing the largest single-district impact (949.92 km² inundated). Cotton damage at Naushahro Feroze (343.98 km² destroyed, 36.7% loss) was particularly alarming given its role as Pakistan's principal cash crop (Qamer et al., 2023). Combined agricultural losses are estimated at US$ 3.7 billion, not accounting for livestock losses (84,271 animals perished) or cascading impacts on food security.

The 2022 flood resulted from unprecedented meteorological conditions. Pakistan received +180% above-normal rainfall, with Sindh province receiving +307% and Balochistan +450% excess precipitation; the highest recorded in 62 years (Qamer et al., 2023). In July-September 2022, Sindh received over 7 times the average rainfall (+726%). The flood was preceded by extreme heatwaves, with daytime temperatures recorded at 2.21ºC above normal in May across several parts of Pakistan (including temperatures exceeding 51ºC on 14 May in Jacobabad). These conditions generated a low-pressure system that attracted moisture-laden winds from the Bay of Bengal and the Arabian Sea and accelerated glacial melting before the monsoon onset, saturating the Indus River system. GRACE-FO observations confirmed the severity through pronounced water equivalent thickness peaks, indicating extended floodwater retention. Rainfall and atmospheric pressure showed significant positive correlation ($p = 0.04$, $r = 0.55$), confirming

the critical role of low-pressure systems (Nazli et al., 2025). The 2022 event involved a persistent low-pressure system over southern Pakistan, representing a shift from the 2010 floods' northern pattern. Nanditha et al. (2023) found that July-early August precipitation saturated the soil, preventing subsurface penetration during late August peak flows. Ashfaq et al. (2023) identified ENSO and La Niña as contributing factors. Similarly, Zafar et al. (2024) observed temperatures of approximately 40ºC in several Pakistani Cities during May. Zafar et al. (2024) also utilized sentinel 1 data to extract flood-inundated crops damaged by the flood. Similar finding were reported by Sarwar et al. (2025b), who also documented precipitation six time above normal, followed by riverine and flash flooding, causing substantial economic losses primarily due to inundation of crops including cotton, rice and sugarcane. F. Roth et al. (2023) reported that maximum inundation extent was observed on 30 August, which aligns closely with the time frame of the current study.

The districts examined demonstrated social and physical vulnerability, as evidenced by previous floods in 2010, 2011, and 2012 (Atif et al., 2021). The Indus Basin has a 7,000-year flooding history, with archaeological evidence suggesting catastrophic floods contributed to ancient civilization decline, including Mohenjo-Daro near Naushahro Feroze. Floodwater remained stagnant for extended periods (up to 4 months in 2011, 3 months in 2012 and 2022) due to poor drainage infrastructure, multiplying the impacts. Although Left Bank Outfall Drain (LBOD) and Right Bank Outfall Drain (RBOD**)** were designed to direct excess water toward the Arabian Sea, they proved inadequately designed for actual discharge volumes (Khaskheli et al., 2024). The Guddu and Sukkur barrages have lost capacity due to siltation and erosion, while riverbank management remains minimal. Under shifting climate patterns, precipitation extremes in South Asia have intensified, making the Indus Basin increasingly vulnerable. Studies by Chen et al. (2024) and Florian Roth et al. (2023) using Sentinel-1 datasets demonstrated the capability of radar-based products for assessing hydro-climatic extreme events where ground truth data are unavailable. This study's reliance on freely available Sentinel-1A SAR data and open-source SNAP tools makes the methodology readily replicable in flood-prone regions globally.

Despite dense road networks, the study area remains vulnerable to disconnection during floods. Bridges that become ineffective during significant flooding link settlements on both Indus River banks, three bridges were damaged: one in Kashmore and two in Naushahro Feroze. Railway lines serve as an economical transportation in remote parts of Sindh, making their disruption particularly devastating. The study area encompasses several historical sites, particularly near the UNESCO World Heritage Site of Mohenjo-Daro in Naushahro Feroze,

requiring careful flood defense management. Damages were exacerbated by water stagnation due to drainage complications, gentle slopes, blockages, and inadequately designed RBOD and LBOD canals (Khaskheli et al., 2024). Prolonged stagnant water significantly hindered restoration of essential services. Across the four districts, 2,548 government buildings suffered damage, disrupting administrative and public services. Regarding the limitations of this research, the temporal resolution of the spatial data represents the primary constraint. It is possible that in the intervening period, a number of houses and government infrastructure have been constructed that are not incorporated in the spatial data, potentially resulting in reduced impact assessment accuracy. Therefore, future researchers should consider validating spatial data and, where necessary, updating it to include all relevant infrastructure elements.

Given the widespread nature of the flood and its related impacts, the government needs to revise its contingency plans and ensure that all remote settlements are included in emergency planning. The government should prioritize shelter locations and ensure that this information is communicated to all residents. During the 2022 flood event, it was observed that the availability of rescue boats was insufficient and should be increased in future emergency preparedness plans. The stockpile of essential medicines must also be increased for such events. A thorough structural inspection of buildings must be conducted to evaluate their resilience and vulnerability to collapse in the event of future flooding.

5. Conclusion

This study demonstrated the effectiveness of Sentinel-1A SAR data processed using SNAP for systematic flood inundation and damage assessment during the August 2022 extreme flood event in Upper Sindh, Pakistan. By applying a histogram-based thresholding approach to dual-polarized SAR imagery, the study successfully delineated flood extents under persistent cloud cover and adverse weather conditions, overcoming the inherent limitations of optical remote sensing during monsoon seasons. The results show that VH polarization consistently provided superior discrimination between flooded and non-flooded surfaces compared to VV polarization, owing to its enhanced sensitivity to surface roughness and vegetation–water interactions. The application of speckle filtering (Lee 3×3) and terrain correction using the SRTM DEM improved spatial coherence while preserving flood boundaries, enabling reliable binary flood classification. Peak inundation mapped on 28 August 2022 covered 1,118.38 km² in Kashmore, 2,144.35 km² in Jacobabad, 1,703.40 km² in Shikarpur, and 1,244.05 km² in Naushahro Feroze, with maximum

flood occurrence concentrated at elevations of 45.72–57.91 m above sea level, highlighting the strong influence of local topography on floodwater accumulation. The spatial flood extent analysis revealed severe multi-sectoral impacts. Agricultural land suffered the most extensive damage, with 5,235 km² inundated across the four districts. Jacobabad experienced the highest proportional agricultural loss (93.12%), followed by Shikarpur (81.72%), Kashmore (76.65%), and Naushahro Feroze (24.21%). Rice cultivation incurred the largest absolute losses (1,788.09 km²), while cotton damage in Naushahro Feroze (343.98 km²; ~36.7%) was particularly critical given its national economic importance. Flood impacts on settlements and infrastructure were equally severe. A total of 1,928 settlements were inundated, affecting 1,859,154 people and causing 258 fatalities within the study area. Transportation networks were extensively disrupted, with 113.08 km of railway lines and 3,171.22 km of roads submerged, severely constraining emergency response and post-flood recovery. Prolonged water stagnation, driven by inadequate drainage capacity and silted barrages , extended inundation durations to several months in some locations, compounding damage to housing, public services , and health infrastructure. This study confirms that Sentinel-1 SAR data combined with open-source SNAP processing provides an operationally viable framework for rapid flood mapping in data-scarce and resource-constrained regions. In the context of intensifying hydro-climatic extremes under climate change — which also pose a significant threat to Pakistan's food security (Abbas et al., 2026; Zafar et al., 2025) — the findings underscore the growing vulnerability of the Indus Basin to compound flood drivers, including extreme monsoonal rainfall, antecedent heatwaves, glacial melt, and structural inadequacies in flood management infrastructure. The approach presented in this study provides actionable spatial evidence that can support early warning and response, damage assessment, and long-term flood risk reduction planning. Furthermore, this approach can be used to calculate tangible and intangible losses, identify sites for new construction and pre-existing vulnerable structures, and assess in advance the potential disruption to critical facilities such as hospitals, factories, and schools. Future work should focus on integrating multi-temporal SAR time series, automated machine-learning classifiers, and multi-sensor data fusion to enhance temporal monitoring, improve classification accuracy, and support near-real-time flood early warning systems for climate-resilient disaster management.

Availability of data

The data that support the findings of this study are available from the corresponding author upon reasonable request.

Conflict of Interest

The authors declare that they have no known competing financial interests or personal relationships that could have appeared to influence the work reported in this paper.

References

Argenti, F., Lapini, A., Bianchi, T., & Alparone, L., 2013, A tutorial on speckle reduction in synthetic aperture radar images. IEEE Geoscience and remote sensing magazine, 1(3): 6-35.

Arif, H., Khan, M., Khan, I. A., Lahori, A. H., & Kausar, A., 2026, Mapping Flood-Prone Areas and Crop Damage Assessment Using Remote Sensing and GIS: A Comparative Analysis of the 2010 and 2022 Floods in Sindh, Pakistan. Journal of the Indian Society of Remote Sensing.

Ashfaq, M., Johnson, N., Kucharski, F., Diffenbaugh, N. S., Abid, M. A., Horan, M. F., Singh, D., Mahajan, S., Ghosh, S., & Ganguly, A. R., 2023, The influence of natural variability on extreme monsoons in Pakistan. npj Climate and Atmospheric Science, 6(1), 148.

Atif, S., Umar, M., & Ullah, F., 2021, Investigating the flood damages in Lower Indus Basin since 2000: Spatiotemporal analyses of the major flood events. Natural Hazards, 108(2): 2357-2383. https://doi.org/10.1007/s11069-021-04783-w

Bates, B., Kundzewicz, Z., & Wu, S., 2008, Climate change and water. Intergovernmental Panel on Climate Change Secretariat.

Chen, F., Zhang, M., Zhao, H., Guan, W., & Yang, A., 2024, Pakistan's 2022 floods: Spatial distribution, causes and future trends from Sentinel-1 SAR observations. Remote sensing of environment, 304, 114055.

Clement, M. A., Kilsby, C. G., & Moore, P., 2018, Multi-temporal synthetic aperture radar flood mapping using change detection. Journal of Flood Risk Management, 11(2): 152-168. https://doi.org/https://doi.org/10.1111/jfr3.12303

CRED, The Centre for Research on the Epidemiology of Disasters, 2024, CRED Publication 2023 Disasters in Numbers - A Significant Year of Disaster Impact. https://www.un-spider.org/. Retrieved May 10, from https://www.un-spider.org/news-and-events/news/cred-publication-2023-disasters-numbers-significant-year-disaster-impact

DeVries, B., Huang, C., Armston, J., Huang, W., Jones, J. W., & Lang, M. W., 2020, Rapid and robust monitoring of flood events using Sentinel-1 and Landsat data on the Google Earth Engine. Remote sensing of environment, 240, 111664.

Fahd, S., Waqas, M., Zafar, Z., Soufan, W., Almutairi, K. F., & Tariq, A., 2025, Integration of RUSLE model with remotely sensed data over Google Earth Engine to evaluate soil erosion in Central Indus Basin. Earth Surface Processes and Landforms, 50(3), e70019. https://doi.org/https://doi.org/10.1002/esp.70019

Ghouri, A. Y., ur Rehman, A., Rasheed, F., Miandad, M., & Rehman, G., 2024, Flood mapping using the Sentinel-1 SAR dataset and application of the change detection approach technique (CDAT) to the Google Earth engine in Sindh province, Pakistan. Ecological Questions, 35(2): 149-159.

Goswami, B. N., Venugopal, V., Sengupta, D., Madhusoodanan, M., & Xavier, P. K., 2006, Increasing trend of extreme rain events over India in a warming environment. Science, 314(5804): 1442-1445.

Gupta, A. K., & Nair, S. S., 2011, Urban floods in Bangalore and Chennai: risk management challenges and lessons for sustainable urban ecology. Current Science, 1638-1645.

Hafeez, S., Guan, M., Munir, B. A., & Yu, D., 2026, Uncovering spatiotemporal patterns of floods using multi-sensor optical and synthetic aperture radar imagery in the major agriculture zone of Sindh, Pakistan. Natural Hazards, 122(7), 288. https://doi.org/10.1007/s11069-026-08057-1

Hong, S., Jang, H., Kim, N., & Sohn, H.-G., 2015, Water area extraction using RADARSAT SAR imagery combined with landsat imagery and terrain information. Sensors, 15(3): 6652-6667.

Jamal, N., & Rahman, A. U., 2026, Evaluating the effectiveness of flood forecasting and early warning system in the diverse topographic region of Indus River Basin, Pakistan using the SWOT approach. Discover Geoscience, 4(1), 110. https://doi.org/10.1007/s44288-026-00477-7

Jensen, J. R., 2009, Remote sensing of the environment: An earth resource perspective 2/e. Pearson Education India.

Jonkman, S. N., Curran, A., & Bouwer, L. M., 2024, Floods have become less deadly: an analysis of global flood fatalities 1975–2022. Natural Hazards, 120(7): 6327-6342. https://doi.org/10.1007/s11069-024-06444-0

Khaskheli, R., Abbasi, M. H., Marvi, H., & Bhutto, A., 2024, The Cause of the Disasters in Sindh: The Failure of LBOD, Incomplete RBOD Project, and Non-functional Old Natural Waterways. Journal of Architecture and Built Environment Research (JABER), 1(1).

Kundzewicz, Z. W., Kanae, S., Seneviratne, S. I., Handmer, J., Nicholls, N., Peduzzi, P., Mechler, R., Bouwer, L. M., Arnell, N., & Mach, K., 2014, Flood risk and climate change: global and regional perspectives. Hydrological Sciences Journal, 59(1): 1-28.

Lavell, A., Oppenheimer, M., Diop, C., Hess, J., Lempert, R., Li, J., & Myeong, S., 2012, Managing the risks of extreme events and disasters to advance climate change adaptation. A special report of working groups I and II of the intergovernmental panel on climate change (IPCC), 3: 25-64.

Lee, J.-S., Jurkevich, L., Dewaele, P., Wambacq, P., & Oosterlinck, A., 1994, Speckle filtering of synthetic aperture radar images: A review. Remote sensing reviews, 8(4): 313-340.

Lee, J., Perera, D., Glickman, T., & Taing, L., 2020, Water-related disasters and their health impacts: A global review. Progress in Disaster Science, *8*, 100123. https://doi.org/https://doi.org/10.1016/j.pdisas.2020.100123

Lillesand, T., Kiefer, R. W., & Chipman, J., 2015, Remote sensing and image interpretation. John Wiley & Sons.

Manjusree, P., Prasanna Kumar, L., Bhatt, C. M., Rao, G. S., & Bhanumurthy, V., 2012, Optimization of threshold ranges for rapid flood inundation mapping by evaluating backscatter profiles of high incidence angle SAR images. International Journal of Disaster Risk Science, 3: 113-122.

McBride, J. L., & Nicholls, N., 1983, Seasonal Relationships between Australian Rainfall and the Southern Oscillation. J Monthly Weather Review, 111(10): 1998-2004. https://doi.org/https://doi.org/10.1175/1520-0493(1983)111<1998:SRBARA>2.0.CO;2

Moazzam, M. F. U., Lee, B. G., Rahman, A. U., Farid, N., & Rahman, G., 2020, Spatio-statistical analysis of flood susceptibility assessment using bivariate model in the floodplain of river swat, district charsadda, Pakistan. Journal of Geoscience and Environment Protection, 8(05), 159.

Mushtaq, F., Ali, M., Ghosh, A., Jalal, R., Asghar, A., Dadhich, G., Chiozza, F., Franceschini, G., Muchoney, D., Toirov, F., Rolle, F., & Henry, M.2022, A rapid geospatial flood impact assessment in Pakistan, 2022. Rome, FAO. https://doi.org/10.4060/cc2873en

Nanditha, J., Kushwaha, A. P., Singh, R., Malik, I., Solanki, H., Chuphal, D. S., Dangar, S., Mahto, S. S., Vegad, U., & Mishra, V., 2023, The Pakistan flood of August 2022: causes and implications. Earth's Future, 11(3), e2022EF003230.

Nazli, S., Liu, J., Song, T., Soomro, S.-e.-h., & Wang, H., 2025, A hybrid machine learning approach to unravel monsoon variability and meteorological dynamics of Pakistan's 2010 and 2022 historic floods. Journal of Hydrology: Regional Studies, 60, 102505. https://doi.org/https://doi.org/10.1016/j.ejrh.2025.102505

NDMA, 2023, Pakistan Flood 2022. Post-Disaster Needs Assessment. Ministry of Planning, Development, and Special Initiatives. https://www.pc.gov.pk/

Niyas, N., Srivastava, A., & Hatwar, H., 2009, Variability and trend in the cyclonic storms over north Indian Ocean. National Climate Centre. Met. Monograph No. Cyclone Warning - 3/2009.

PDMA Sindh, 2022, Flood 2022 in Sindh. https://pdma.gos.pk/Documents/Reports/Flood%202022%20In%20Sindh.pdf

Pham-Duc, B., Prigent, C., & Aires, F., 2017, Surface water monitoring within Cambodia and the Vietnamese Mekong Delta over a year, with Sentinel-1 SAR observations. *Water*, *9*(6), 366.

Qamer, F. M., Abbas, S., Ahmad, B., Hussain, A., Salman, A., Muhammad, S., Nawaz, M., Shrestha, S., Iqbal, B., & Thapa, S., 2023, A framework for multi-sensor satellite data to evaluate crop production losses: the case study of 2022 Pakistan floods. Scientific Reports, 13(1), 4240. https://doi.org/10.1038/s41598-023-30347-y

Rahman, G., Anwar, M. M., Ahmed, M., Ashraf, H., & Zafar, U., 2017, Socio-economic damages caused by the 2014 flood in Punjab Province, Pakistan: Socio-economic damages caused by the 2014 flood in Punjab. Proceedings of the Pakistan Academy of Sciences: B. Life and Environmental Sciences, 54(4): 365–374.

Romero, C., 2010, High resolution simulation of synthetic aperture radar imaging. California Polytechnic State University.

Roth, F., Bauer-Marschallinger, B., Tupas, M. E., Reimer, C., Salamon, P., & Wagner, W. (2023). Sentinel-1-based analysis of the severe flood over Pakistan 2022. Nat. Hazards Earth Syst. Sci., 23(10): 3305-3317. https://doi.org/10.5194/nhess-23-3305-2023

Roth, F., Bauer-Marschallinger, B., Tupas, M. E., Reimer, C., Salamon, P., & Wagner, W., 2023, Sentinel-1-based analysis of the severe flood over Pakistan 2022. Natural Hazards and Earth System Sciences, 23(10): 3305-3317.

Roxy, M. K., Ritika, K., Terray, P., Murtugudde, R., Ashok, K., & Goswami, B., 2015, Drying of Indian subcontinent by rapid Indian Ocean warming and a weakening land-sea thermal gradient. Nature communications, 6(1), 7423.

Sarwar, J., Khan, S. A., Azmat, M., Khan, F., & Javed, S., 2025a, A GIS-based technique for estimation of economic losses from riverine flood in the lower Indus basin. Natural Hazards, 122(1), 31. https://doi.org/10.1007/s11069-025-07876-y

Sarwar, J., Khan, S. A., Azmat, M., Khan, F., & Javed, S. (2025b). A GIS-based technique for estimation of economic losses from riverine flood in the lower Indus basin. Natural Hazards, 122. https://doi.org/10.1007/s11069-025-07876-y

Sindh, G. O., 2022, Sindh Statistics 2022. Retrieved from https://sohris.com/sindh-statistics-2022

Sivasankar, T., Das, R., Borah, S. B., & Raju, P., 2019, Insight to the potentials of Sentinel-1 SAR data for embankment breach assessment. Proceedings of International Conference on Remote Sensing for Disaster Management: Issues and Challenges in Disaster Management, p. 33-41. https://doi.org/10.1007/978-3-319-77276-9

Twele, A., Cao, W., Plank, S., & Martinis, S., 2016, Sentinel-1-based flood mapping: a fully automated processing chain. International Journal of Remote Sensing, 37(13): 2990-3004.

UNDRR, 2011, Revealing Risk, Redefining Development: The 2011 Global Assessment Report on Disaster Risk Reduction. https://www.undrr.org/quick/11179

Villarini, G., Serinaldi, F., Smith, J. A., & Krajewski, W. F., 2009, On the stationarity of annual flood peaks in the continental United States during the 20th century. Water Resources Research, 45(8).

Xia, S., Ruan, R., Yan, M., & She, Y., 2011, Extraction of Hongze Lake reclamation area based on RADARSAT SAR and LANDSAT ETM+. Procedia Environmental Sciences, 10: 2294-2300.

Zafar, Z., Fahd, S., Zubair, M., Zulqarnain, R. M., & Abbas, Q., 2026, Evaluating the InVEST model to map water ecosystem services in the data-scarce upper Indus basin. Acta Geophysica, 74(2), 124. https://doi.org/10.1007/s11600-026-01848-x

Zafar, Z., Zubair, M., & Fahd, S., 2024, Extreme weather events and their socioeconomic impacts: A remote sensing-based analysis of flood damages. Global and Earth Surface Processes Change, 1, 100001. https://doi.org/https://doi.org/10.1016/j.gespch.2024.100001

Zeng, L., Schmitt, M., Li, L., & Zhu, X. X., 2017, Analysing changes of the Poyang Lake water area using Sentinel-1 synthetic aperture radar imagery. International Journal of Remote Sensing, 38(23): 7041-7069.